The Chemical Kinetics for the Reaction of O(³P) with Ethylene

Jong-Tae Lim, Kyoung-Yong Cho, Chang-Yul Choi, Ho-Rim Park, Joong-Gill Choi*, and Simon H. Bauer†

Department of Chemistry, Yonsei University, Seoul 120-749, Korea
†Department of Chemistry, Baker Laboratory, Cornell University, Ithaca, New York 14853, U.S.A.
Received February 10, 1995

The kinetics of the reaction between O(³P) and C_2H_4 was investigated by measuring time-dependent concentrations of OH resulting from the reaction by using the LIF detection. Oxygen atoms were generated by titrating microwave discharged N_2/He with NO to the chemiluminescent end point. The operating pressures in the flow reactor ranged from 5 to 15 torr and the mixtures consisted of He/O(³P)/C_2H_4 in the approximate ratios from 100/1/0.1 to 100/1/1. The controlled residence time prior to the detection were estimated to be 0.8-17 ms at the reactor pressure of 7 torr. Experimentally determined profiles both in shape and magnitude were compared with the computed OH density for a specified set of experimental parameters, allowing us to arrive at a complete mechanism for the reaction of O(³P) with ethylene.

Introduction

During the last few decades, the importance in the reactions of fuels with O(³P) and OH(²Π$_i$) has been well recognized in the field of the combustion and atmospheric chemistry. In many fuel types encountered in combustion environments, hydrocarbons consist of the vast majority. Therefore the availability of large amounts of elementary kinetic data[1] and improved techniques for estimating specific reaction rates have contributed to the increasing application of the detailed chemical kinetic modeling as an important tool in the analysis of these systems. Consequently, extensive studies for these reactions have led not only to the measurement of the rate constants but also to the investigation of the reaction mechanisms involved.

The mechanism for the reaction of O(³P) with saturated hydrocarbons has been suggested to undergo through a simple hydrogen abstraction. Recently, Cohen and Westberg[2] have reported a current summary for oxygen-atom attack on alkanes. In earlier reviews assembled by Herron and Huie,[3,4] it has been found that the rates of H abstraction by O(³P) in alkanes are in the order of primary>secondary>tertiary and the total rates have been approximately predicted as the sum of the rates of the individual C-H bonds.[5] There is a total agreement in these literatures that the primary products are alkyl radicals and OH. In addition, the abstraction of H atoms from alkanes by OH radicals reviewed by Atkinson *et al.*[6~8] follows a similar pattern to that by O atoms.

A general feature of the kinetic measurements such as the evaluation of rate coefficients have been conducted under conditions in which one species is in excess over the other to minimize the complications resulting from secondary or tertiary reactions. However it has been pointed out by Cohen[9] that in alkane+O(³P) reactions, the measured values are especially sensitive to errors caused by uncounted secondary reactions and impurities in the reagents. He also has assembled a detailed model consisting of 27 and 44 separated reactions for oxidation of CH_4 and C_2H_6, respectively. Under most conditions for the CH_4+O(³P) system, he has concluded that it can be simplified by including 13 reactions. Recent report by Borchardt *et al.*[10] has discussed the reactions of O(³P) with B_2H_6 and C_2H_6 by measuring the time-dependent concentrations of OH and quantitatively evaluating the experimental data with a computer simulation. It shows that at least 29 and 40 elementary reactions must be included to understand complete kinetic mechanisms for ethane and diborane with ground-state atomic oxygens, respectively.

It has been known that ethylene is a primary fuel itself and is produced in large amounts during the combustion of saturated hydrocarbons such as CH_4, C_2H_6, etc.. There have been several studies assembled to provide a detailed comprehensive reaction mechanism for the ethylene combustion.[11] It has been demonstrated that the elementary reactions of C_2H_4 and its products are somewhat different from the properties of alkane fuels. Detailed discussions of chemical kinetic modeling of hydrocarbon oxidation including ethylene under combustion conditions have been reviewed by Westbrook and Dryer.[11] In addition, several results have been reported on theoretical[12,13] and experimental[14~17] investigations for the reaction of ethylene with O(³P). It seems that although many features of ethylene combustion have begun to be resolved, other details still remain uncertain.

The laser-induced fluorescence (LIF) detection has become a direct method to investigate the dynamics of quantum-selected states of electronically-excited molecules including free radicals. This technique has been used to study the dynamics of hydrogen abstraction reactions of hydrocarbons with O(³P) atoms by measuring OH($X^2\Pi$) produced.[18~20] It is evident that until rates of production of specific species are determined, overall mechanisms cannot be established. In this report we present time-dependent OH concentrations generated under a certain condition to describe the kinetics of the reaction of excess O(³P) with ethylene. The products of a fast-flow reactor were sampled *via* LIF by OH. The fluorescence intensities for runs were measured under strictly comparable conditions. Computational simulations were carried out and the time-dependent concentrations were compared with the experimental values. As a consequence, the best estimates for the rate coefficients at the temperature

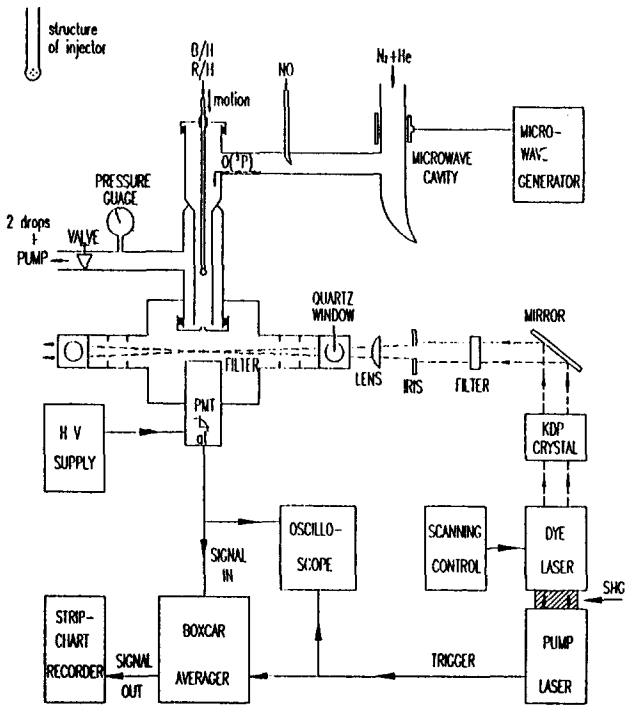

Figure 1. Schematics of experimental configuration.

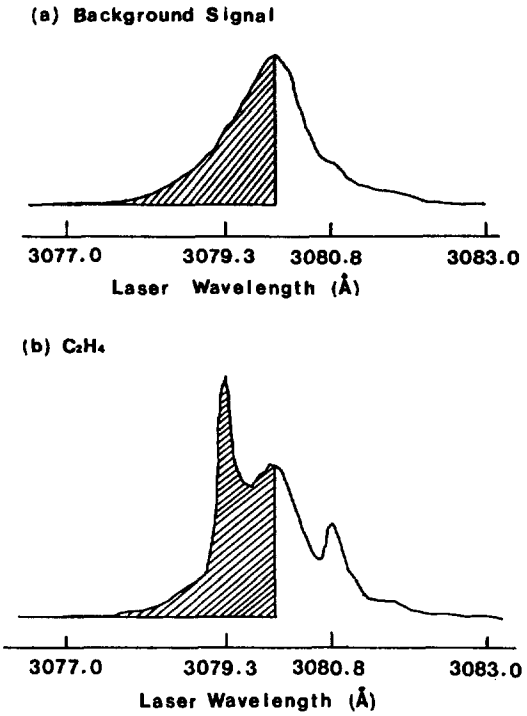

Figure 2. Typical scans of LIF signals: (a) Background signal; (b) C_2H_4 (20% mole fraction in Ar) signal.

of the flow medium and overall reaction mechanism can be determined, which is in the vicinity of 350 K based on the rotational temperature determined in a similar flow system.[21]

Experimental

A block diagram displaying the experimental arrangements of the LIF used in this investigation is shown in Figure 1, which is basically same as that described previously.[10] The light source used in the setup consisted of a pulsed dye laser (Quanta-Ray PDL-1), using a sulforhodamine 101 dye, which was pumped by a Nd : YAG laser (Quanta-Ray DCR) with a repetition rate of 10 Hz. The output of the dye laser was frequency doubled with a KDP crystal to produce a maximum pulse energy of about 1 mJ at 308 nm and a bandwidth of approximately 0.1 nm FWHM. The laser was tuned to the (0, 0) band of $Q_1(1)$ transition of $OH(A^2\Sigma^+ - X^2\Pi)$ system occuring at 307.8 nm. The excitation was filtered by a visible light rejection filter and focused onto the well-defined reaction zone by a lens. The entrance and exit of the beam were formed by quartz windows at the Brewster angle. The fluorescence signal was detected by a combination of EMI 6256B photomultiplier and UV glass filter (Hoya 4340) rejecting wavelengths outside the region 275-375 nm at right angle with respect to the direction of the laser beam and OH radicals sampled. The output signal from the PMT was electronically processed and averaged through a boxcar integrator (PARC model 160) with a gate width of 5 μs delayed by 0.5 μs. The signal from the boxcar averager was then recorded on a strip chart recorder.

The ground state oxygen atoms were produced by a visual titration method where N_2 in the mixture of N_2+He was dissociated by a microwave discharge and followed by the titration with NO. A stream of O atoms free of O_2 generated from above procedure was then introduced into the reaction region through a side arm of reactor tube. The rates of the gas flow were monitored by a series of metering valves and flow meters, which were calibrated by measuring the rates of pressure decrease in known volumes. The samples of C_2H_4 mixed with He were eluted through a thin and long Pyrex tube of 0.63 cm i.d. located inside of the Pyrex reactor of 2.5 cm (upper part) and 1.25 cm (lower part) in diameter with a 30 cm in length. The thin sample injecting tube could be slid along the axis of the reactor to displace the mixing region relative to the sampling pinhole of 0.50 mm.

The pressure in the reactor was controlled and maintained at 1-15 torr, depending on the opening of the valve connected with a fast mechanical pump. The reaction products expanded under near-continuum flow through the skimmer (0.75 mm in diameter) into the detection region. In the typical experimental condition where the total pressure in the reactor was maintained at 7 torr, the flow rates of the gases were found to be 2.30 μmol/s and 0.17 μmol/s for O and C_2H_4, respectively. The linear flow speed of the sample was calculated to be 2.1×10^3 cm/s, so that the shortest dwell time in the reactor, which corresponded to the reaction time, was about 0.8 ms. The longest time could be extended to 17 ms at the reactor pressure of 7 torr and to 35 ms at 14 torr. From the fact that the concentration of C_2H_4 was about 10 times less than that of O atoms, it could be assumed all the samples of C_2H_4 react with oxygen atoms. It gave rise to the elimination of any secondary reactions due to C_2H_4 remaining after the initial reaction. Note that the background pressure in the detection area was kept at less than 10^{-3} torr in conjunction with a 10 cm oil diffusion pump.

The stock gases used in these studies were obtained from

AIRCO for N_2 (99.995%), He (99.995%), and Ar (99.998%), from Matheson for NO (cp, 99.0% min), and from MG Scientific Gases for C_2H_4 (cp, 99.5% min). The NO gas was purified by trap-to-trap distillation prior to use. In order to check the levels of impurities in the sample, ethylene was injected onto a FID gas chromatograph and no detectable impurity was found in the gas sample.

For a fixed orientation of the KDP crystal, a broad background signal (Figure 2a) was recorded (with no C_2H_4 flow) when the dye laser output was scanned over a 0.3 nm on either side of 307.9 nm. It was demonstrated that beyond the bandwidth of the crystal there was no detectable fluorescence intensity. When OH was generated by the reaction between ethylene and excess O(^{3}P), the OH fluorescence spectrum appeared to be superposed on this background (Figure 2b). The sharp line features were assigned as indicated: Q_1 (1) at 307.93; Q_1(2) at 308.09 nm. The fluorescence intensity developed at a selected transition can be changed by rotating the doubling crystal to maximize the laser power at the desired resonance frequency.

In view of the constant low levels of exciting radiation quenching effects were negligible. It was assumed that the differences in the integrated areas of the scans when ethylene was injected and the background were direct measures of the ground state populations of OH present in the sampling jet. To minimize possible perturbations of relative yields of different product states the integrations were carried out only over the $Q_1(1)$ resonance from $\lambda = 307.7$ nm to the maximum of the background signal (indicated by the shaded areas in Figure 2). Each set of records was integrated seven times; the largest and smallest readings were discarded and a mean was taken of the remaining five. Several runs were repeated for each set of conditions. Standard deviations for each integration and each run were found to be <3% and 5%, respectively.

Results and Discussion

At first, in order to ensure that the measurements for the reaction rate were achieved within the region where the signal responded linearly to the concentration of the sample, OH signals were recorded as varying the flow rate of C_2H_4. It was found that the dependence of fluorescence yields showed the linear increase with the relative flow rate of the sample. Secondly, all the experimental parameters such as laser intensity, flow rates, and operating pressures were kept constant, except for varing the position of the sample injection tube. Thus the relative fluorescence intensities deduced from the differences in the recorded areas were direct measures of the relative amounts of OH($^2\Pi_i$) generated in the flow reactor at corresponding residence times.

The reaction time was determined by the overall gas flow rate and the location of the fuel injector relative to the sampling pinhole giving rise to 1-35 ms time range for residence prior to sampling in practice. The amplifier/boxcar-integrated currents of the LIF signals from OH were converted to absolute intensities at the sampling pinhole by equating the observed signal to that calculated with the best set of rate constants. Based on the procedure by Borchardt *et al.*,[10] the calibration was justified by assuming that the imposed condition for an acceptable mechanism was that the computed

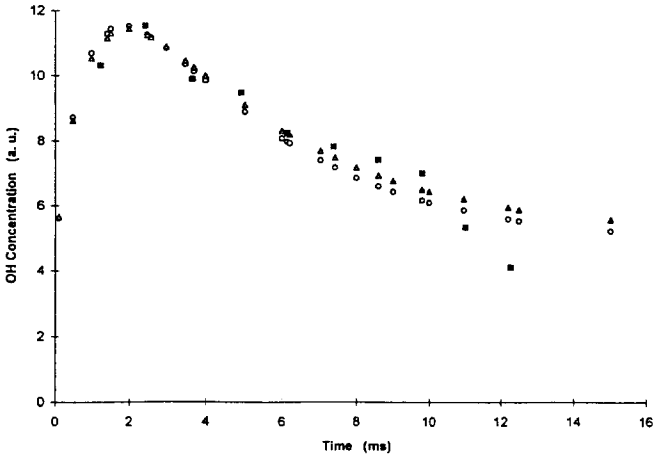

Figure 3. Concentration of OH with respect to the reaction time, observed (■) *vs* calculated (○; 31 Reactions used, △; 131 reactions used).

time dependent shapes for OH signals match those observed experimentally.

The calculations carried out to simulate actual experimental results include the compilation of most plausible 131 reactions needed to describe the evolution of the systems O(^{3}P) with C_2H_4. The initial concentrations of reactants were calculated from the measurements of flow rates to give 2.02×10^{-7} mole/L for ethylene and 2.57×10^{-6} mole/L for O(^{3}P) at the reactor pressure of 7 torr. The C_2H_4/O(^{3}P) ratio was then varied from 0.1 to 1.0 for different experimental conditions. Note that in the reactor the major constituent was helium at about 5×10^{-4} mol/L so that the reactants were present at roughly 1/100 of that level.

The expanded kinetics code[22] used here requires only that the reacting species be specified, their reactions listed, and for each a rate constant inserted. The computer then prints out: (a) the concentration of each of the species as a function of time; (b) the net rates of conversion of each species as a function of time; (c) the Jacobian for a selected species relative to all the others at selected times; i.e. in our case, $d\{\partial[OH]/\partial t\}/d[X]$. This provides a direct measure of the sensitivity of the species of interest to inclusions of other species and of any plausible reactions. With this scheme total of 50 species and 200 reaction rates can be integrated. Figure 3 shows that, by normalizing the computed to the observed intensitiy at 6.14 ms, both runs are well reproduced over the entire reaction period from 0 ms to 15 ms for the reactor pressure of 7 torr.

In our experimental conditions, the significant initial steps for the $O+C_2H_4$ reaction

$$C_2H_4 + O \longrightarrow \begin{cases} C_2H_3 + OH & \text{(R1)} \\ CH_3 + HCO & \text{(R2)} \\ CH_2 + HCHO & \text{(R3)} \\ CH_2CHO + H & \text{(R4)} \end{cases}$$

are followed by many elementary processes. A detailed model consisting of 42 species, which participated in possible 131 reactions including above reactions, had been assembled and simulated to generate the calculated graphs. It soon became evident that for the conditions in our experiments only 19 species were essential and the number of reactions was

Table 1. A Minimal Mechanism for $C_2H_4+(^3P)$ Reactions

No.	Reactants	Products	k (L/mols)	Comment
R1	C_2H_4+O	$=C_2H_3+OH$	8.50E02	
R2	C_2H_4+O	$=CH_3+HCO$	2.35E08	(a)4.9E08
R3	C_2H_4+O	$=CH_2+HCHO$	5.70E06	(a)5.7E06
R4	C_2H_4+O	$=CH_2CHO+H$	1.00E07	
R5	$O+OH$	$=HO_2$	4.25E08	b, d
R6	$O+OH$	$=O_2+H$	2.60E10	b, c
R7	$O+H$	$=OH$	1.80E07	b, d
R8	$O+HO_2$	$=OH+O_2$	3.75E10	b, (e)3.75E10
R9	$H+OH$	$=H_2O$	4.14E08	b, c
R10	$H+O_2$	$=HO_2$	4.56E06	b, (f)7.06E06
R11	$H+HO_2$	$=H_2+O_2$	8.00E09	b, (g)3.11E09
R12	$H+HO_2$	$=OH+OH$	3.89E10	b, c
R13	$H+HO_2$	$=H_2O+O$	1.81E09	
R14	$H+H$	$=H_2$	4.50E06	c, (b)2.50E06,
R15	C_2H_4+OH	$=CH_3+HCHO$	3.20E09	(a)4.0E08, (h)3.2E09
R16	C_2H_4+OH	$=CH_3CHO+H$	2.50E09	(h)2.5E09
R17	C_2H_4+OH	$=C_2H_3+H_2O$	6.10E08	(a)6.1E08
R18	CH_3CHO+O	$=CH_3CO+OH$	4.50E08	b, d
R19	$CH_3CHO+OH$	$=CH_3CO+H_2O$	1.00E10	
R20	CH_3CHO+H	$=CH_3CO+H_2$	3.47E07	a
R21	CH_3CO+O	$=CH_3+CO_2$	3.00E10	b, d
R22	CH_3+O	$=HCHO+H$	2.00E11	(b)1.00E11
R23	CH_3+H	$=CH_4$	2.00E10	
R24	CH_2+O	$=CO+H_2$	5.01E09	a
R25	$HCO+O$	$=H+CO_2$	7.50E10	b, (c)3.0E10
R26	$HCO+O$	$=OH+CO$	2.68E10	b, (c)3.0E10
R27	$HCO+H$	$=CO+H_2$	6.60E10	b, (i)8.43E10
R28	$HCHO+H$	$=HCO+H_2$	4.00E07	b, (c)3.46E07
R29	$HCHO+O$	$=HCO+OH$	2.19E08	b, c
R30	$HCHO+OH$	$=H_2O+HCO$	5.60E09	b, (c)6.09E09
R31	$CO+OH$	$=CO_2+H$	9.15E07	a

[a]Reference 11, [b]Reference 10, [c]Reference 25, [d]Reference 23, [e]Reference 27, [f]Reference 28, [g]Reference 29, [h]Reference 9, [i]Reference 30

reduced to 31, as listed in Table 1. These reactions were selected by three criterions from the computer output as mentioned above. It was found that the concentrations of each species at the time scale of interest were within 10% of those calculated with the larger set (131 reactions). It should be pointed out that there are 10 reactions (R5 to R14) which are very sensitive and important to control the time-dependent concentrations of OH. These are part of the H/O system which are usually present in all low pressure and low temperature flames for hydrogenic fuels. The rate constants of these reactions were unaltered from those used in reference 10.

In addition to these steps, the rate constants used for the computation were picked as the most reasonable values from refs. 1, 3, 9, 11, 24, and 26. The rate constants inserted in the code are those listed in the available tables or are estimates based on analogous reactions. They are subjected to reasonable revisions as requested to obtain fits between the computed time dependent OH concentrations and those observed, as well as of their absolute magnitudes. For three-body reactions (R5, R7, R9, R10, R14, and R23), corresponding two-body rate constants were obtained by multiplying the three-body values by 3.8×10^{-4} mole/L (*i.e.* the concentration of M in this experiments for a reactor pressure of 7 torr). Note that there is no room temperature data available for the radical reactions R5, R7, and R9 and these values are somewhat larger than those reported for higher temperature. This is reasonable providing that transition-state thoery predict a negative temperature dependence for termolecular associations with small or zero activation energies.[10,25]

It should be pointed out that the reported data of the rate coefficients for those system were varied by even several orders of magnitude for certain cases. Many small changes in the magnitudes of several rate constants were made and the computation was continued until the best fits between experiments and calculations were obtained. The rate constants for the most sensitive reactions (R1, R2, R5, R7, R9, and R16) remained within an order of magnitude of the literature values. Note that relative reaction rate sensitivities among R1, R2, R5, R7, R9, and R16 at 3 ms, for instance, were calculated to be 1.000, 0.025, 0.994, 1.669, 0.026, and 0.812, respectively. At other time scales, these numbers varied slightly, however, the relative reaction sensitivities still remained at similar values within the time ranges of 0-30 ms. Most of the other rate constants, which were important to describe but not as much sensitive as those six reactions, were kept fixed during the curve fitting. Figure 3 shows the computed and the observed intensities of [OH] in time for $C_2H_4+O(^3P)$ reaction. It demonstrates the results are well reproduced over the entire reaction period from 0 ms to 15 ms for He reactor pressure of 7 torr. Note that reduced set of the reactions (31 reactions) reproduces the almost same profile of OH concentration as that of larger set (131 reacrions). Some descrepancies between the observed and calculated signals at the higher time scale are believed to result from the unstable fluorescence signals.

As shown in Table 1, OH is generated in the reactions R1, R7, R8, R12, R18, R26, and R29 and destroyed in the reactions R5, R6, R9, R15, R16, R17, R19, R30, and R31. However, it is notable that at early stage reactions R1 and R7 are the major sources for the production and R5, R6, and R16 for the consumption of OH radicals. In addition, H atoms and HO_2 radicals play an important role to control the OH concentration in later time scale. During the entire reaction period of interest in our investigation, in deed, an extended computer model consisting of 31 steps shows that the steady state concentration of OH is controllled by several rate processes;

$$[OH]_{SS}\simeq\frac{\Sigma_i k_i[R_i][O]+\Sigma_j k_j[R_j][H]}{(k_5+k_6)[O]+(k_{15}+k_{16}+k_{17})[C_2H_4]+\Sigma_r k_r[R_r]}$$

$$\simeq(k_5+k_6)^{-1}\times\frac{\Sigma_i k_i[R_i]+\Sigma_j k_j[R_j]\{[H]/[O]\}}{[1+\{(k_{15}+k_{16}+k_{17})/(k_5+k_6)\}\{[C_2H_4]/[O]\}+\Sigma_r\{k_r/(k_5+k_6)\}\{[R_r]/[O]\}]}$$

$$\simeq(k_5+k_6)^{-1}\frac{\alpha+\beta}{1+\gamma+\delta}$$

where

R_i=C_2H_4, H, HO_2, CH_3CHO, HCO, HCHO,
R_j=HO_2, and
R_r=H, CH_3CHO, HCHO, and CO.

Using the computational results we can calculate the parameter α, β, γ, and δ. At 7 torr operating pressure and 10 ms residence time, these values were determined to be α= 15.60 s^{-1}, β=3.552×10^{-1} s^{-1}, γ=7.009×10^{-4} s^{-1}, and δ= 1.094×10^{-2} s^{-1}.

In addition to the initial steps (R1-R4), channel to produce H_2+CH_2CO is thermodynamically possible.[23] However, it is unlikely to be the major route for the products channels for $O+C_2H_4$ reaction based on analogous reaction such as $H+C_2H_4$. Smalley *et al.*[16] reported that the branching ratio for $H+C_2H_3O$ (vinoxy) product channel had the values of 0.27± 0.05. Note that the addition reactions (R2, R3, and R4) generally have smaller activation energies than the abstraction reactions (R1) so that at room temperature R1 is often negligibly slow, but under high temprature conditions the abstraction reactions can be very important.[11] The results from the computer simulation show indeed that the hydrogen abstraction reaction, R1, is insensitive to the variation of OH concentrations within the time scale of this experiment. The rate constants for abstraction reactions reported in the table were selected to provide the best fits between the computed and observed magnitudes and shape of the time-dependent OH concentrations.

It is interesting to note that the graphs and the mechanism in general are analogous to those for $C_2H_6+O(^3P)$ system reported by Borchardt *et al.*,[10] even though the initiating steps of R1 to R4 for the reaction of $O(^3P)$ with C_2H_4 are unique. Moreover, the reactions required in all H/O system which are very sensitive to the OH profiles in time are also included with the same values of rate constants as those in $C_2H_6+O(^3P)$. Conclusively, the propriety of the mechanism in this report can be found in the fact that it has included all data set essential for the reaction kinetics of $C_2H_4+O(^3P)$ and the selection of pertinent reactions are based on the literatures. Then the best estimates for a minimal mechanism have been reduced, providing the most rate constants listed within the reasonable revisions from the reported values in the vicinity of room temperatures.

Conclusion

We have presented time-dependent concentration of OH resulting from the reaction of $O(^3P)$ with C_2H_4 *via* LIF. The experimental results on OH profiles along with the model calculations provide the best estimates for the reaction mechanism including the rate coefficients. It also demonstrates that many elementary reactions must be taken into account in order to elucidate the oxidation kinetics of ethylene. This fact still applies even when the oxygen/hydrocarbon ratio is relatively large. In addition, it seems that small changes in the proposed rate constants do not affect the shapes of the OH profiles. In order to conclude the mechanisms regarding the oxidation reaction of ethylene, more sophistigated diagnostics for assaying the resultant radical compositions and the investigations of rate constants for each steps as much detail as possible are demanded. In conclusion, it is instructive to recall that the concepts of this work possess strong implications for further extension of the reaction kinetics and the determination of rate constants in a dynamics for not only the combustion chemistry but also many related fields.

Acknoledgment. This research was financially supported by the Korea Research Foundation (1989) and Basic Science Research Program, Ministry of Education, Republic of Korea.

References

1. Herron, J. T.; Huie, R. E. *J. Phys. Chem.* **1973**, Ref. Data 2, 467.
2. Cohen, N.; Westberg, K. R. *Int. J. Chem. Kin.* **1986**, *18*, 99.
3. Huie, R. E.; Herron, J. T. *Prog. React. Kin.* **1975**, *8*, 1.
4. Herron, J. T.; Huie, R. E. *J. Phys. Chem.* **1969**, *73*, 3327.
5. Luntz, A. C.; Andresen, P. *J. Chem. Phys.* **1980**, *72*, 5851.
6. Atkinson, R.; Darnall, K. R.; Winer, A. M.; Lloyd, A. C.; Pitts, J. N., Jr. *Advances in Photochemistry*; Vol. 11, p 375-488, edited by Pitts, J. N., Jr.; Hammond, G. S.; Gollnick, K., Wiley: New York, U.S.A., 1979.
7. Atkinson, R. *Int. J. Chem. Kin.* **1986**, *18*, 555.
8. Droege, A. T.; Tully, F. P. *J. Phys. Chem.* **1986**, *90*, 1949.
9. Cohen, N. *Int. J. Chem. Kin.* **1982**, *14*, 1339.
10. Borchardt, D. B.; Choi, J. G.; Suzuki, K.; Bauer, S. H. *J. Chem. Phys.* **1988**, *88*, 6282.
11. Westberg, C. K.; Dryer, F. L. *Prog. Energy Combust. Sci.* **1984**, *10*, 1.
12. Harding, L. B.; Wagner, A. F. *J. Phys. Chem.* **1986**, *90*, 2974.
13. Dupuis, M.; Wendoloski, J. J.; Takada, T.; Lester, W. A., Jr. *J. Chem. Phys.* **1982**, *76*, 481.
14. Davis, D. D.; Huie, R. F.; Herron, J. T.; Kurylo, M. J.; Braun, W. *J. Chem. Phys.* **1972**, *56*, 4868.
15. Peeters, J.; Schaekers, M.; Vinckier, C. *J. Phys. Chem.* **1986**, *90*, 6552.
16. Smalley, J. F.; Nesbitt, F. L.; Klemm, R. B. *J. Phys. Chem.* **1986**, *90*, 491.
17. Koda, S.; Endo, Y.; Hirota, E.; Tsuchiya, S. *J. Phys. Chem.* **1987**, *91*, 5840.
18. Dutton, N. J.; Fletcher, I. W.; Whitehead, J. C. *J. Phys. Chem.* **1985**, *89*, 569.
19. Kleinermanns, K.; Luntz, A. C. *J. Chem. Phys.* **1982**, *77*, 3533.
20. Dutton, N. J.; Fletcher, I. W.; Whitehead, J. C. *Mol. Phys.* **1984**, *52*, 475.
21. Jeffers, P. M.; Bauer, S. H. *J. Phys. Chem.* **1984**, *88*, 5039.
22. The kinetic code, H1CHM, was developed by W. Braun at National Bureau of Standards (Gaithersburg, Maryland, U.S.A.) and expanded by Dr. N. S. Chiu at Cornell University in several respects.
23. Sridharan, W. C.; Kaufman, F. *Chem. Phys. Lett.* **1983**, *102*, 45.
24. Westley, F. *Table of Recommended Rate Constants for Chemical Reactions Occuring in Combustions, Natl. Bur. Stand. Ref. Data. Ser.*; Washington, D.C., U.S. GPO, 1980.
25. Moore, J. W.; Pearson, R. G. *Kinetics and Mechanism*; Chaps. 5 and 6, Wiley: New York, U.S.A., 1981.
26. Tsang, W.; Hampson, R. F. *J. Phys. Chem.* **1986**, Ref. Data

15, 1087.
27. Vicovich, J. M.; Wine, P. H. *J. Phys. Chem.* **1987**, *91*, 5118.
28. Hsu, K. J.; Durant, J. L.; Kaufman, F. *J. Phys. Chem.* **1987**, *91*, 1895.
29. Baulch, D. L.; Cox, R. A.; Hampson, R. F.; Jr., Kerr, J. A.; Troe, J.; Watson, R. *J. Phys. Chem.* **1984**, Ref. Data 13, 1259.
30. Timonen, R. S.; Ratajczak, E.; Gutman, D. *J. Phys. Chem.* **1987**, *91*, 692.

Studies of Nonstoichiometry and Physical Properties of the Perovskite $Sm_{1-x}Sr_xCoO_{3-y}$ System

Jin Woo Kang, Kwang Hyun Ryu, and Chul Hyun Yo

Department of Chemistry, Yonsei University, Seoul 120-749, Korea

Received February 16, 1995

A series of samples in the $Sm_{1-x}Sr_xCoO_{3-y}$ (x=0.00, 0.25, 0.50, 0.75 and 1.00) system has been prepared at 1200 ℃ under ambient atmosphere. The X-ray diffraction patterns of the samples with x=0.00 and 0.25 are indexed with orthorhombic symmetry like $GdFeO_3$ and x=0.50 appears to be perfectly cubic. In the tetragonal system (x=0.75), the structure is similar to that of $SrCoO_{2.80}$. The composition of x=1.00, $SrCoO_{2.52}$, shows the brownmillerite-type structure. The reduced lattice volume is increased with x value in this system. The chemical analysis shows the τ value (the amount of the Co^{4+} ions in the system) is maximized at the composition of x=0.50. Nonstoichiometric chemical formulas are determined by the x, τ and y values. The electrical conductivity has been measured in the temperature range of 78 to 1000 K. The activation energy is minimum for those of x=0.25 and x=0.50 with metallic behavior. First-order semiconductor-to-metal transition of $SmCoO_3$ is not observed. Instead, a broad, high-order semiconductor-to-metal transition is observed. In general, the effective magnetic moment is increased with increasing τ values at low temperature. At high temperature, the magnetic moment is maximum for that of x=0.00. The 3d-electrons are collective and give ferromagnetism in x=0.50.

Introduction

Preparations and characterizations of oxides containing appreciable quantities of cobalt in a rare valence state +4 have been reported by several research groups. In perovskite-type ABO_3 compounds, the higher valence state of the transition metal is generally stabilized with larger A-site ion.[1~7]

Raccah and Goodenough[8] and Bhide *et al.*[9] have investigated a $LaCoO_3$ system in which cobalt ions predominantly exist in the diamagnetic, low spin state $Co^{3+}(t_{2g}^6e_g^0)$ at low temperature. According to these studies, the low-spin $^1A_1$ state of trivalent cobalt ion is only 0.08 eV more stable than the high-spin $^5T_2$ state. Therefore, the equilibrium between the states can be changed with temperature. They have also suggested that $LaCoO_3$ exhibits a first-order transition due to the delocalization of the eg electrons forming a σ^* band states. So beyond 1200 K, $LaCoO_3$ becomes metallic.

Thornton *et al.*,[10] however, have suggested that the $LnCoO_3$ (Ln : La, Nd, Gd, Ho, and Y) system show broad, high order semiconductor-to-metal transitions over the approximate temperature ranges (La : 385-570 K, Nd : 400-590 K, Gd : 490-770 K). These transitions involve gradual delocalization of eg electron to form a collective σ^* band.

The $SrCoO_{2.5}$ has brownmillerite or hexagonally deficient perovskite structure depending on annealing temperature and oxygen pressure during the sample preparation.[11~13] The high temperature phase of $SrCoO_{2.5}$ is brownmillerite-type, orthorhombic structure, and has the Néel temperature of 550 K.[11]

Substitution of La^{3+} in $LaCoO_3$ by Sr^{2+} (creating Co^{4+} holes) brings about remarkable changes.[13,14] Thus, the system $La_{1-x}Sr_xCoO_3$ becomes ferromagnetic at low temperatures when x>0.125, the ferromagnetism arising from the positive Co^{4+}-O-Co^{3+} interaction; the d electrons show itinerant behavior (both above and below T_c) in these compositions.

In this present study, the $Sm_{1-x}Sr_xCoO_{3-y}$($0.00 \le x \le 1.00$) system has been prepared and their structures are analyzed by X-ray diffraction and a thermal analysis method. The amount of Co^{4+} ions to the total cobalt ions is determined by an iodometric titration. The magnetic and other physical properties of this system with the nonstoichiometry are discussed.

Experimental

Samples of $Sm_{1-x}Sr_xCoO_3$ with various values of x (x=0.00, 0.25, 0.50, 0.75, and 1.00) were prepared by coprecipitating the starting materials in the required proportions, essentially following the method described earlier.[16] The starting materials were Sm_2O_3, $SrCO_3$, and $Co(NO_3)_2 \cdot 6H_2O$. Appropriate amounts of the mixtures were dissolved in dilute nitric acid. The solution was evaporated over a burner flame and then fired at 800 ℃ for 4 hr. After being ground, the samples were heated at 1200 ℃ under an ambient atmosphere for